

## The Interaction of the Rieske Iron-Sulfur Protein with Occupants of the Q<sub>o</sub>-site of the bc<sub>1</sub> Complex, Probed by Electron Spin Echo Envelope Modulation\*

Received for publication, November 19, 2001,  
and in revised form, December 13, 2001  
Published, JBC Papers in Press, December 17, 2001,  
DOI 10.1074/jbc.C100664200

Rimma I. Samoilova‡, Derrick Kolling§,  
Taketoshi Uzawa¶, Toshio Iwasaki||,  
Antony R. Crofts§, and Sergei A. Dikanov‡\*\*\*‡‡

From the ‡Institute of Chemical Kinetics and Combustion, Russian Academy of Sciences, Novosibirsk 630090, Russia, the §Department of Biochemistry, University of Illinois, Urbana, Illinois 61801, the ¶Division of Natural Science, Osaka Kyoiku University, Osaka 582-8582, Japan, the ||Department of Biochemistry and Molecular Biology, Nippon Medical School, Tokyo 113-8062, Japan, and the \*\*\*Illinois EPR Research Center and Department of Veterinary Clinical Medicine, University of Illinois, Urbana, Illinois 61801

The bifurcated reaction at the Q<sub>o</sub>-site of the bc<sub>1</sub> complex provides the mechanistic basis of the proton pumping activity through which the complex conserves redox energy in the proton gradient. Structural information about the binding of quinone at the site is lacking, because the site is vacant in crystals of the native complexes. We now report the first structural characterization of the interaction of the native quinone occupant with the Rieske iron-sulfur protein in the bc<sub>1</sub> complex of *Rhodobacter sphaeroides*, using high resolution EPR. We have compared the binding configuration in the presence of quinone with the known structures for the complex with stigmatellin and myxothiazol. We have shown by using EPR and orientation-selective electron spin echo envelope modulation (ESEEM) measurements of the iron-sulfur protein that when quinone is present in the site, the isotropic hyperfine constant of one of the N<sub>δ</sub> atoms of a liganding histidine of the [2Fe-2S] cluster is similar to that observed when stigmatellin is present and different from the configuration in the presence of myxothiazol. The spectra also show complementary differences in nitrogen quadrupole splittings in some orientations. We suggest that the EPR characteristics, the ESEEM spectra, and the hyperfine couplings reflect a

similar interaction between the iron-sulfur protein and the quinone or stigmatellin and that the N<sub>δ</sub> involved is that of a histidine (equivalent to His-161 in the chicken mitochondrial complex) that forms both a ligand to the cluster and a hydrogen bond with a carbonyl oxygen atom of the Q<sub>o</sub>-site occupant.

The cytochrome (cyt)<sup>1</sup> bc<sub>1</sub> complex family plays an essential role in the energy metabolism of the biosphere (1, 2), providing the central enzymes in the electron transfer chains of all the major pathways. In bacteria, and their mitochondrial and chloroplasts descendants, the complex catalyzes oxidation of quinol and reduction of a diffusible small protein (cyt *c* or *c*<sub>2</sub> in  $\alpha$ -proteobacteria) through a modified Q-cycle (3–6).

Interest in the bc<sub>1</sub> complex has been heightened by the recent availability of structures and the new insights into functional aspects that these have encouraged (2, 7–12). However, with the structures has come the realization that the static models do not provide all the information needed to understand mechanism at a deeper level. The reactions of greatest interest are the proton-coupled electron transfers at the quinone-processing sites. In particular, oxidation of ubiquinol at the Q<sub>o</sub>-site of the complex is the key reaction of the Q-cycle, providing the bifurcation of electron transfer between two different acceptor chains that allows coupling to proton transfer. The Q<sub>o</sub>-site of the mitochondrial complex, and its mechanism, are also of central importance to the physiology of cellular damage and aging, because it is a major site for generation of reactive oxygen species.

To understand the mechanism, we need detailed information about the local reaction environment, including protein structure, hydrogen bonding, and distances, to provide the parameters that control rates, and partitioning of electrons to different pathways. Of the five well characterized paramagnetic centers of the bc<sub>1</sub> complex that are formed during different partial reactions, the most studied is the [2Fe-2S] cluster of the Rieske iron-sulfur protein (ISP), the EPR signal of which was found to vary with the redox state of the quinone pool, and inhibitor occupancy of the Q<sub>o</sub>-site (13–18).

Interaction of the Q<sub>o</sub>-site inhibitors stigmatellin and UHDBT with the Rieske cluster occurs via formation of a hydrogen bond with the His-161, which is one of the iron ligands of the reduced cluster (7–12). Although none of the crystallographic structures shows any occupancy of the site by the substrate ubihydroquinone (quinol, QH<sub>2</sub>), or the product ubiquinone (quinone, Q), much biophysical evidence had suggested that both these native occupants interact with the ISP through a similar configuration (2, 13–18). Previous applications in the g<sub>y</sub> region found minor effects of inhibitors on the ESEEM spectra of UHDBT-treated mitochondrial bc<sub>1</sub> complex (19), and DBMIB-treated b<sub>6</sub>f complex isolated from spinach chloroplasts (20). No conclusions

\* This work was supported by National Institutes of Health Grant GM35438 (to A. R. C.); NATO Grant 977132 (to A. R. C. and R. S.); National Science Foundation Grant DBI-9602240 (to D. K.); National Science Foundation Grant INT-9910113 (to S. A. D.); Ministry of Education, Science, Sport and Culture of Japan Grant-in-aid 1169237, and Japan-United States Cooperative Science Program Grant from JSPS BSAR-507 (to T. I.). The costs of publication of this article were defrayed in part by the payment of page charges. This article must therefore be hereby marked "advertisement" in accordance with 18 U.S.C. Section 1734 solely to indicate this fact.

‡‡ Supported by Illinois EPR Research Center (National Institutes of Health Grant RR01811). To whom correspondence should be addressed: Illinois EPR Research Center, University of Illinois, Urbana, IL 61801. E-mail: dikanov@uiuc.edu.

<sup>1</sup> The abbreviations used are: cyt, cytochrome; bc<sub>1</sub> complex, the ubihydroquinone:cytochrome *c* oxidoreductase (EC 1.10.2.2); ESEEM, electron spin echo envelope modulation; HYSCORE, hyperfine sublevel correlation; sq, single-quantum transition; dq, double-quantum transition; UHDBT, 5-*n*-undecyl-6-hydroxy-4,7-dioxobenzothiazole; DBMIB, 2,5-dibromo-6-methyl-3-isopropyl-1,4-benzoquinone; Q and QH<sub>2</sub>, quinone and quinol, respectively, forms of ubiquinone-10; ISP (ISP<sub>ox</sub> and ISP<sub>red</sub>), Rieske iron-sulfur protein (oxidized and reduced forms).

TABLE I

A. Characteristics of the EPR spectra of the $bc_1$ complex with different $Q_o$ -site occupants								
Sample	$g_z (\pm 0.003)$	$g_y (\pm 0.003)$	$g_x (\pm 0.005)$	$g_z - g_y$	$g_y - g_x$	$g_z - g_x$	$R_z (\%)$	$R_x (\%)$
$bc_1$ + myxothiazol	2.028	1.896	1.758	0.132	0.138	0.270	103	97
$bc_1$ + quinone	2.020	1.890	1.803	0.130	0.087	0.217	75	128
$bc_1$ + stigmatellin	2.020	1.886	1.783	0.134	0.103	0.237	83	118

B. Components of hyperfine tensors $A_i (\pm 0.1$ MHz) along the g-tensor axes and isotropic hyperfine couplings calculated for two coordinated nitrogens.								
Sample	$A_z$		$A_y$		$A_x$		$A_{iso}$	
	$N_{\delta 1}$	$N_{\delta 2}$						
$bc_1$ + myxothiazol	4.3	4.3	4.9	3.7	5.0	4.0	4.7	4.0
$bc_1$ + quinone	5.2	4.2	5.1	3.8	4.9	3.9	5.1	4.0
$bc_1$ + stigmatellin	5.4	4.3	5.0	3.8	5.3	4.5	5.2	4.2

were drawn about possible interactions of the inhibitors with the cluster or changes in geometry of ligands.

In this paper we describe initial studies using high resolution pulsed EPR to explore the involvement of the reduced ISP ( $ISP_{red}$ ) in formation of the enzyme-product (EP) complex at the  $Q_o$ -site and in changes in conformation in response to the inhibitors stigmatellin and myxothiazol as alternative occupants of the site. We have used orientation-selective ESEEM experiments to quantify these effects through the hyperfine couplings of the reduced cluster with nitrogens of the coordinated histidines. We demonstrate the first quantitative characterization of the influence of the  $Q_o$ -site occupants on the distribution of electron spin density over the ligands and the geometry of their coordination.

#### EXPERIMENTAL PROCEDURES

**Sample Preparation**—Recombinant wild-type cyt  $bc_1$  complex having the His-tag at the C terminus of cyt  $b$  subunit (BH6) was homologously overproduced in *Rhodospirillum rubrum* cells and purified in a single-step purification procedure as described previously (21). This protocol yields an active enzyme containing four polypeptides, three to four ubiquinones, and the four redox cofactors in their stoichiometric ratios. The purified enzyme ( $\sim 20 \mu M$  per monomer) was immediately concentrated using Centrion (Amicon Inc., Beverly, MA) concentrators with a cutoff of 100,000 Da at 4 °C. Where added, all inhibitors were present in  $\sim 9.4$ -fold excess concentration over the cyt  $bc_1$  monomer. The following samples, each containing 0.01%  $n$ -dodecyl- $\beta$ -D-maltoside (Sigma), 15  $\mu g/ml$  phosphatidylcholine, and 20% glycerol (added as a cryoprotectant), and antimycin (to eliminate the  $Q_i$ -site semiquinone), were reduced by 10 mM ascorbate, buffered at pH 7.0, and stored at  $-80$  °C until use: the form with native occupant (quinone) (0.60 mM cyt  $c_1$ ), the stigmatellin-bound form (0.31 mM), and the myxothiazol-bound form (0.42 mM).

**EPR Experiments**—EPR measurements were carried out using X-band Bruker ESP-380E spectrometer equipped with Oxford CF 935 cryostats, at 9 K. In ESEEM experiments one-dimensional three-pulse and two-dimensional four-pulse sequences were used as described in detail elsewhere (22, 23).

#### RESULTS AND DISCUSSION

**EPR Spectra**—EPR spectra of reduced samples of  $bc_1$  complex with different occupants of the  $Q_o$ -site show the typical anisotropic lines characteristics of a rhombic g-tensor. The most noticeable difference between the spectra is in the position and width of the  $g_x$  component (13–18, 24), which decreases from  $\sim 1.803$  in  $bc_1$  complex with quinone at the  $Q_o$ -site, to 1.783 with stigmatellin, or 1.758 with myxothiazol. Variations of the two other g-tensor components are less significant but readily detectable. The g-tensors correspond well with previously reported values for similar samples; in addition, we note that the values in the presence of myxothiazol are similar to those for the proteolyzed ISP head domain (24). The g-tensor principal values of  $ISP_{red}$ , and other derived parameters, are summarized in Table IA.

Changes of g-tensor for Rieske clusters have been analyzed in terms of a ligand-field model of the orbitals of the  $Fe^{2+}$  ion in the reduced clusters (25, 26). The theory describes the variation of g-tensor in terms of a mixing of the lowest and highest  $d$ -orbitals, and a phenomenological angular function,  $\theta$ , changes in which were associated with distortion of  $Fe^{2+}$  ligand field. The differences observed for the EPR spectra of the samples used in this study correspond to a variation of  $\theta \sim 1^\circ$ . However, this cannot be attributed to any specific structural changes of the cluster (26).

An alternative approach describes the differences between spectra using two parameters,  $R_z$  and  $R_x$ , derived from the measured principal values of the g-tensor system through the following equation (19, 27).

$$R_{z(x)} = \frac{300(g_y - g_{x(z)})}{(2g_{z(x)} - g_y - g_{x(z)})} (\%) \quad (\text{Eq. 1})$$

The values of  $R_z$  and  $R_x$  depend on the complete width of the spectra characterized by  $g_z - g_x$ , and by the  $g_z - g_y$  and  $g_y - g_x$  splittings (Table IA).  $R_z$  and  $R_x$  are equal (with a value of 100%) when  $g_y - g_x = g_z - g_y$ . A surplus of the left part over the right part leads to  $R_z > 100\%$  and  $R_x < 100\%$  and vice versa. Link (24) has suggested that such a transformation of the spectra, and corresponding variations of  $R_z$  and  $R_x$ , might result from a change from z to x in the unique principal axis of the ligand field coordinate system.

Analysis of the spectra (Table IA) using this approach shows that the  $ISP_{red}$  in the complex with quinone or stigmatellin has values for  $R_z$  and  $R_x$  that are opposite (relative to the 100% border) to the values in the presence of myxothiazol.

This could be interpreted as a switch in orientation of the unique principal axis in these two cases as a result of a variation in the strength of interaction of the  $Q_o$ -site occupants with the reduced cluster, which differentially affects the ligand field and possibly the ligand geometry around the  $Fe(II)$  ion.

**ESEEM Spectroscopy**—To investigate the interaction of the  $Q_o$ -site occupants with the  $ISP_{red}$  in greater detail, we have applied ESEEM spectroscopy to measure the hyperfine couplings between the cluster and the nitrogens of coordinated histidine ligands. For each sample, the three-pulse ESEEM and HYSCORE patterns were collected at three different magnetic fields, corresponding to the singularities of the g-tensor principal values in EPR spectra. Measurement of echo envelopes at different points in the anisotropic EPR spectrum selects iron-sulfur clusters with different orientations of the g-tensor relative to the applied magnetic field.

Fig. 1 shows the superimposed plots of three-pulse ESEEM spectra (frequencies  $< 10$  MHz) of  $ISP_{red}$  for three  $bc_1$  complex samples. The spectra contain a set of lines in the region 0–8 MHz attributable to local interaction with  $^{14}N$  nitrogens (19,

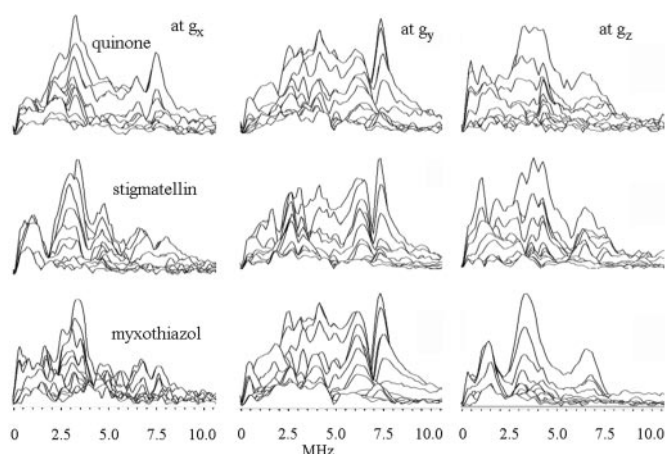


FIG. 1. X-band three-pulse ESEEM spectra of  $ISP_{red}$  in the presence of different  $Q_o$ -site occupants: *top*, quinone; *middle*, stigmatellin; *bottom*, myxothiazol. In each spectrum, antimycin was also present to displace the  $Q_o$ -site occupant. Spectra are displayed as the modulus of the Fourier transform along time  $T$  axis recorded near the  $g_x$  region (*left*),  $g_y$  (*center*), or  $g_z$  (*right*). The initial  $\tau$  is 88 ns in the farthest trace, increased by 24 ns in the successive traces. Microwave frequency was 9.712 GHz.

20, 28). The data in Fig. 1 clearly indicate an orientation dependence of the spectra that arises from excitation of clusters differently oriented with respect to the field. As a result, at both edges ( $g_x$  and  $g_z$  regions) of the EPR spectra, the intensity of the ESEEM lines in the region 5–8 MHz is significantly less than the intensity of lower frequency peaks. In contrast, in the central part ( $g_y$  region) the peaks at 5–8 MHz are comparable with those at low frequencies. The position of the highest frequency peak changes by about  $\sim 0.5$  MHz, which is greater than the variation caused by choice of magnetic field.

Comparison of the ESEEM spectra obtained for the three samples shows other obvious differences, especially at  $g_x$  and  $g_z$ . Features of note in the spectra at  $g_x$  include the variation of the relative intensities of two components with highest frequencies at 7.0 and 7.7 MHz, the enhancement of the line at 5 MHz in the sample with stigmatellin, and clear variations of the shapes of spectral lines at frequencies  $< 4.5$  MHz. Differences of a similar magnitude were observed when the field was in the  $g_z$  region. These are clearly seen as variations of the maximal position and line shape of the highest component with frequency between 6.5 and 7.5 MHz and alterations of the spectral shape at  $< 5$  MHz. In contrast the spectra at the  $g_y$  line showed only marginal variations (in the region  $< 5$  MHz), in confirmation of previous reports (19, 20).

The difference between the samples were also seen in the nitrogen HYSCORE spectra, which provide cross-correlations between different transitions of each nitrogen nucleus from opposite electron spin manifolds, and help in their assignment (28). They resolve also the anisotropy of nuclear transitions that are especially useful in testing whether the ESEEM spectral variations are associated with either the nuclear frequencies or their intensities.

Previous analysis of ESEEM spectra of the Rieske cluster has been interpreted as showing major contributions from the two  $N_\delta$  nitrogens of histidine ligands directly coordinating Fe(II) ion (Fig. 3). There are also possible weak contributions of the  $N_\epsilon$  histidine nitrogens and nitrogens of the protein peptide groups at frequencies  $< 4.5$  MHz (19, 20, 24, 28). Each nitrogen can produce up to six lines in ESEEM spectrum corresponding to two single-quantum (sq) and one double-quantum (dq) transitions from  $m_S = \pm 1/2$  manifolds.

The lines with maximal frequencies in three-pulse spectra correspond to dq transitions ( $\nu_{dq+}$ ) from the  $m_S = +1/2$  manifold

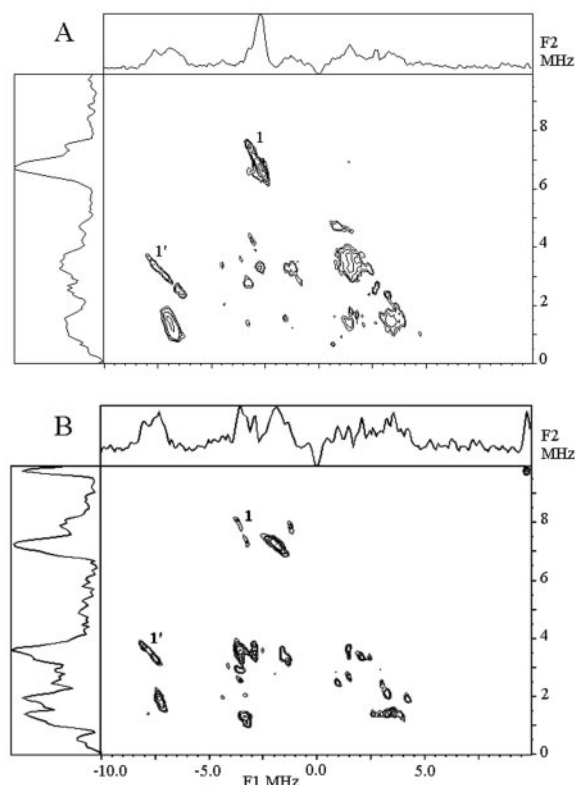


FIG. 2. Comparison of two-dimensional ESEEM (HYSCORE) spectra of reduced  $[2Fe-2S]$  cluster in  $bc_1$  complex with stigmatellin (*top*) and myxothiazol (*bottom*). Excitation was at the  $g_x$  line. Myxothiazol (microwave frequency 9.717 GHz,  $\tau = 128$  ns). Stigmatellin (microwave frequency 9.711 GHz,  $\tau = 128$  ns).

of two  $N_\delta$  nitrogens (22, 28). The dq transitions from the  $m_S = -1/2$  manifold, ( $\nu_{dq-}$ ), have smaller values, with a difference less than  $4\nu_1$  ( $\nu_1$  is the Zeeman frequency of the  $^{14}N$  nucleus) for each nitrogen. Assignment of these transitions from three-pulse spectra is problematic because of the complex character of the spectra. This was resolved by using HYSCORE spectra, which produce easily recognizable cross-peaks with coordinates corresponding to ( $\nu_{dq+}$ ) and ( $\nu_{dq-}$ ) in the  $(+ -)$  quadrant. Fig. 2 shows a comparison of HYSCORE spectra of the reduced  $[2Fe-2S]$  cluster in the complexes with stigmatellin (A) or myxothiazol (B), measured at  $g_x$ . There are different intensities of all cross-peaks in the  $(+ -)$  quadrant of the spectra. The cross-peaks spread around (3.4, 1.5) MHz (indicated by 1 and 1') present in the  $(+ +)$  quadrant of the spectrum with stigmatellin are dominant features. In contrast there are only weak traces of these peaks in the spectrum with myxothiazol.

From a combined analysis of three-pulse and HYSCORE spectra, we were able to assign pairs of dq transitions for both  $N_\delta$  nitrogens for the three samples at different field settings. Using the frequencies of the dq transitions, one can estimate the diagonal elements of the nitrogen hyperfine tensor,  $A_i$ , in the  $g$ -tensor coordinate system from the second-order expressions for  $\nu_{dq\pm}$  frequencies suggested in Ref. 29,  $A_i = 2\nu_1(\nu_{dq+} + \nu_{dq-})/[(8\nu_1) - (\nu_{dq+} - \nu_{dq-})]$  ( $i = x, y, \text{ or } z$ ). Values for  $\nu_{dq\pm}$  are taken from the corresponding spectra obtained near  $g_x$ . Among two values of  $A_i$  found for each orientation of magnetic field, the larger value must always be assigned to one nitrogen ( $N_\delta 1$ ) and smaller one to another ( $N_\delta 2$ ), as shown by electron nuclear double resonance data with  $^{15}N$ -labeled Rieske proteins (30).

The data of Table IB show variation of  $A_i$  in samples with different  $Q_o$ -site occupants, either through variation in the distribution of the unpaired spin density or through a change in the geometry of ligation. Both these effects appear to contribute

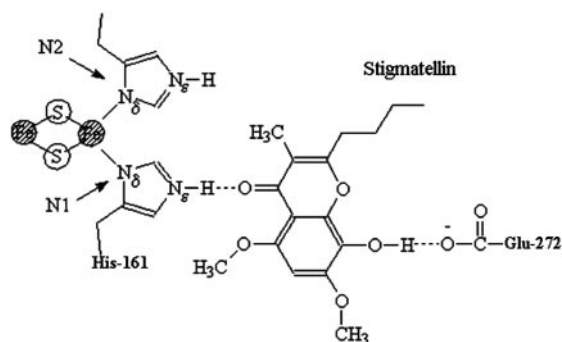


FIG. 3. Schematic representation of the complex formed between stigmatellin and His-161 of the ISP, showing suggested involvement of groups discussed in the text.

to the differences seen on interaction with the different occupants.

Direct information about the unpaired  $2s$  orbital spin density on the nitrogen follows from the isotropic hyperfine constant (22), which is equal  $A_{\text{iso}} = (A_x + A_y + A_z)/3$  (Table IB). The point of particular interest is the increase  $\sim 10\%$  of the  $A_{\text{iso}}$  on  $N_{\delta 1}$ , but not on  $N_{\delta 2}$ . The change of  $\sim 0.5$  MHz is significantly greater than the range of scatter for the experiment.

The three-pulse ESEEM spectrum of  $bc_1$  with myxothiazol at  $g_z$  shows a triplet with frequencies 6.8, 3.4, and 1.7 MHz produced by two  $N_{\delta}$ -atoms magnetically equivalent along this direction. This spectrum provides two sets of nuclear frequencies, at 6.8, 3.4, and 3.4 MHz and at 3.4, 1.7, and 1.7 MHz (confirmed by HYSORE data), which are an indication of zero quadrupole splitting along  $g_z$  for both nitrogens. No equivalence between these nitrogens is found for the samples with stigmatellin or quinone at either  $g_z$  or  $g_x$ , so this difference in symmetry between the two  $N_{\delta}$ -atoms cannot be attributed to a switch of unique axis. The multiple lines indicate the presence of quadrupole splittings from at least one nitrogen along these axes. Because the orientation of the  $N_{\delta}$  quadrupole tensor is associated with the orientation of the imidazole ring, this demonstrates a change in orientation of a histidine in these samples compared with that in the complex with myxothiazol.

**Biochemical Relevance**—In the structure of the  $bc_1$  complex with stigmatellin, the hydrogen bond ( $\sim 2.8$  Å in the yeast complex, 1e2v) involves the carbonyl oxygen of stigmatellin, and the  $N_{\epsilon}$  of His-161, which provides a ligand to the cluster through  $N_{\delta}$ . This interaction (Fig. 3) confirmed a large body of previous physicochemical evidence, suggesting a liganding between  $\text{ISP}_{\text{red}}$  and UHDBT or stigmatellin (reviewed in Refs. 2 and 24). In contrast, in the myxothiazol structure, the  $[2\text{Fe}-2\text{S}]$  cluster of the ISP is found 19 Å away, rotated close to its other reaction interface on cytochrome  $c_1$ , with His-161 exposed to the aqueous phase. This is in line with the absence of evidence for any interaction between ISP and this inhibitor.

The  $N_{\delta 1}$  nitrogen at which the changes identified above occur likely belongs to His-161, the iron ligand that is also involved in the interaction with the  $Q_o$ -site occupants. The similarities of the EPR spectral characteristics, and of the isotropic hyperfine couplings, strongly suggest that quinone has a liganding similar to that seen with stigmatellin (6, 7, 11). Because the formation of the hydrogen bond can be expected to withdraw electron density from the cluster, the change in the spin density at  $N_{\delta}$  of His-161 can be explained by modulation through the strength of the hydrogen bonding configuration at  $N_{\epsilon}$ .

In contrast to previous reports, our experiments have shown marked changes in one-dimensional and two-dimensional ESEEM spectra with change in  $Q_o$ -site occupant, especially when measured in the  $g_x$  and  $g_z$  regions. These initial results provide the first direct structural information on a catalytically relevant state of the  $Q_o$ -site and show that the liganding of quinone with  $\text{ISP}_{\text{red}}$  in the EP complex is similar to that of stigmatellin. More detailed measurements and a more quantitative analysis of the spectra will provide a deeper understanding of the structural changes in the environment of the cluster on binding of quinone or inhibitors.

**Acknowledgments**—Spectroscopic measurements were performed in the Environmental Molecular Sciences Laboratory National Users Facility sponsored by the Department of Energy Office of Biological and Environmental Research and located at Pacific Northwest National Laboratory. We thank Dr. M. K. Bowman for help with EPR experiments.

#### REFERENCES

- Cramer, W. A., Soriano, G. M., Ponomarev, M., Huang, D., Zhang, H., Martinez, S. E., and Smith, J. L. (1996) *Annu. Rev. Plant Physiol. Plant Mol. Biol.* **47**, 477–508
- Berry, E., Guergova-Kuras, M., Huang, L.-S., and Crofts, A. R. (2000) *Annu. Rev. Biochem.* **69**, 1007–1077
- Mitchell, P. (1976) *J. Theor. Biol.* **62**, 327–367
- Crofts, A. R., Meinhardt, S. W., Jones, K. R., and Snozzi, M. (1983) *Biochim. Biophys. Acta* **723**, 202–218
- Crofts, A. R. (1985) *The Enzymes of Biological Membranes* (Martonosi, A. N., ed) Vol. 4, pp. 347–382, Plenum Publishing Corp., New York
- Crofts, A. R., Hong, S. J., Ugulava, N., Barquera, B., Gennis, R. B., Guergova-Kuras, M., and Berry, E. (1999) *Proc. Natl. Acad. Sci. U. S. A.* **96**, 10021–10026
- Zhang, Z., Huang, L.-S., Shulmeister, V. M., Chi, Y.-I., Kim, K.-K., Hung, L.-W., Crofts, A. R., Berry, E. A., and Kim, S.-H. (1998) *Nature (Lond.)* **392**, 677–684
- Xia, D., Yu, C.-A., Kim, H., Jia-Zhi Xia, J.-Z., Kachurin, A. M., Zhang, L., Yu, L., and Deisenhofer, J. (1997) *Science* **277**, 60–66
- Iwata, S., Lee, J. W., Okada, K., Lee, J. K., Iwata, M., Rasmussen, B., Link, T. A., Ramaswamy, S., and Jap, B. K. (1998) *Science* **281**, 64–71
- Kim, H., Xia, D., Yu, C. A., Xia, J. Z., Kachurin, A. M., Zhang, L., Yu, L., and Deisenhofer, J. (1998) *Proc. Natl. Acad. Sci. U. S. A.* **95**, 8026–8033
- Hunte, C., Koepke, J., Lange, C., Roßmanith, T., and Michel, H. (2000) *Structure (Lond.)* **8**, 669–684
- Yu, C.-A., Xia, D., Kim, H., Deisenhofer, J., Zhang, L., Kachurin, A., and Yu, L. (1998) *Biochim. Biophys. Acta* **1365**, 151–158
- Ding, H., Moser, C. C., Robertson, D. E., Tokito, M. K., Daldal, F., and Dutton, P. L. (1995) *Biochemistry* **34**, 15979–15996
- Ding, H., Robertson, D. E., Daldal, F., and Dutton, P. L. (1992) *Biochemistry* **31**, 3144–3158
- De Vries, S., Albracht, S. P. J., Berden, J. A., and Slater, E. C. (1982) *Biochim. Biophys. Acta* **681**, 41–53
- De Vries, S., Albracht, S. P. J., Berden, J. A., Marres, C. A. M., and Slater, E. C. (1983) *Biochim. Biophys. Acta* **723**, 91–103
- Crofts, A. R., Barquera, B., Gennis, R. B., Kuras, R., Guergova-Kuras, M., and Berry, E. A. (1999) *Biochemistry* **38**, 15807–15826
- Crofts, A. R., Guergova-Kuras, M., Kuras, R., Ugulava, N., Li, J., and Hong, S. (2000) *Biochim. Biophys. Acta* **1459**, 456–466
- Shergill, J. K., and Cammack, R. (1994) *Biochim. Biophys. Acta* **1185**, 35–42
- Britt, R. D., Sauer, K., Klein, M. P., Knaff, D. B., Kriauciunas, A., Yu, C. A., Yu, L., and Malkin, R. (1991) *Biochemistry* **30**, 1892–1901
- Guergova-Kuras, M., Salcedo-Hernandez, R., Bechmann, G., Kuras, R., Gennis, R. B., and Crofts, A. R. (1998) *Protein Expression Purif.* **15**, 370–380
- Dikanov, S. A. (2000) *New Advances in Analytical Techniques* (Atta-ur-Rahman, ed) pp. 536–586, Gordon and Breach, Amsterdam
- Höfer, P., Grupp, A., Nebenfür, H., and Mehring, M. (1986) *Chem. Phys. Lett.* **132**, 279–284
- Link, T. A. (1999) *Adv. Inorg. Chem.* **47**, 83–157
- Bertrand, P., Guigliarelli, B., Gayda, J.-P., Beardwood, P., and Gibson, J. (1985) *Biochim. Biophys. Acta* **831**, 261–266
- Bertrand, P., Guigliarelli, B., and More, C. (1991) *New J. Chem.* **15**, 445–454
- Blumberg, W. E., and Peisach, J. (1974) *Arch. Biochem. Biophys.* **162**, 502–512
- Dikanov, S. A., Xun, L., Karpel, A. B., Tyryshkin, A. M., and Bowman, M. K. (1996) *J. Am. Chem. Soc.* **118**, 8408–8416
- Dikanov, S. A., Tyryshkin, A. M., Hüttermann, J., Bogumil, R., and Witzel, H. (1995) *J. Am. Chem. Soc.* **117**, 4976–4985
- Gurbiel, R. J., Doan, P. E., Gassner, G. T., Macke, T. J., Case, D. A., Ohnishi, T., Fee, J. A., Ballou, D. P., and Hoffman, B. M. (1996) *Biochemistry* **35**, 7834–7845